European Journal of Medicinal Chemistry 225 (2021) 113734

Contents lists available at ScienceDirect

European Journal of Medicinal Chemistry

journal homepage: http://www.elsevier.com/locate/ejmech

Novel C-3-(*N*-alkyl-aryl)-aminomethyl rifamycin SV derivatives exhibit activity against rifampicin-resistant *Mycobacterium tuberculosis* $RpoB_{S522L}$ strain and display a different binding mode at the RNAP β-subunit site compared to rifampicin

Mire Zloh [a, b], Megha Gupta [c], Tanya Parish [d], Federico Brucoli [e, *]

[a] *Faculty of Pharmacy, University Business Academy, Novi Sad, 2100, Serbia*
[b] *UCL School of Pharmacy, UCL, London, WC1N 1AX, UK*
[c] *Infectious Disease Research Institute, 1616 Eastlake Ave E, Suite 400, Seattle, WA, 98102, USA*
[d] *Center for Global Infectious Disease Research, Seattle Children's Research Institute, 307 Westlake Avenue North, Suite 500, Seattle, USA*
[e] *Leicester School of Pharmacy, De Montfort University, Leicester, LE1 9BH, UK*

ARTICLE INFO

Article history:
Received 12 April 2021
Received in revised form
26 July 2021
Accepted 28 July 2021
Available online 8 August 2021

Keywords:
Rifampicin analogues
Tuberculosis drug discovery
Reductive amination
Anti-microbial drug resistance
Medicinal chemistry
Molecular modelling

ABSTRACT

Antimicrobial resistance is a main concern in tuberculosis treatment and is often associated with the emergence of *Mycobacterium tuberculosis* strains resistant to rifampicin (RIF), which is one of the cornerstones of tuberculosis chemotherapy. In this study, aminoalkyl-aromatic ring tails were appended to the C3 position of rifamycin core to assess the role of C3 substitutions to the anti-mycobacterial activity of the rifamycin antibiotics. The typical hydrazone unit of RIF was replaced by an amino-alkyl linkage to connect the aromatic ring tails with the rifamycin naphthoquinone core. Eight novel C3-(*N*-alkyl-aryl)-aminoalkyl analogues of rifamycin SV were synthesised and screened *in vitro* against wild-type HR37Rv and "hypervirulent" HN-878 strains, and a panel of rifampicin-resistant *M. tuberculosis* clinical isolates carrying mutations at the 522, 531 and 455 positions of the *rpoB* gene ($RpoB_{S522L}$, $RpoB_{S531L}$ and $RpoB_{H455D}$ strains). The analogues exhibited anti-tubercular activity against H37Rv and HN-878 at submicromolar or nanomolar concentrations, and against clinical H37Rv isolates bearing the S522L mutations at low micromolar concentration. Benzylamine moiety-including analogue **8** was as active as rifampicin against HN-878 with a MIC_{90} value of 0.02 μM, whereas **14** and **15**, which included tryptamine and *para*-methyl-sulfonylbenzylamine C3-substituents, respectively, showed higher anti-tubercular activity (MIC_{90} = 3 μM) compared to rifampicin against the S522L mutated H37Rv strain. Detailed *in silico* analysis of different RNAP molecular systems predicted a distinct, possibly novel, binding mode for the new rifamycin analogues. These were found to occupy a different space in the binding pockets of both wild type and mutated RNAP proteins compared to that of rifampicin. Moreover, the molecular modelling experiments investigated the ability of the novel analogues aromatic tails to establish key interactions at the RNAP binding site. These interesting findings might pave the way for generating rifamycin analogues that can overcome anti-microbial resistance in *M. tuberculosis*.

1. Introduction

The rifamycins are *ansa* antibiotics (ansamycins) originally isolated from fermentation cultures of *Amycolatopsis rifamycinica* (previously mistakenly identified as *Streptomyces mediterranei*) [1,2]. This family of bacterial secondary metabolites consists of seven molecules, rifamycins A, B, C, D, E, S and SV, which, since their discovery, showed enormous potential as broad-spectrum antimicrobials and anti-tuberculosis agents [3,4].

Rifamycins B (**1**) and SV (**2**) were the first members of this family to enter clinical trials as intravenous antibiotics, although these compounds were found to be chemically unstable *in vivo* due their benzoquinone core and showed some degrees of organ toxicity after parental administration [5].

Several chemical modifications were subsequently carried out at the rifamycin C-3 side chain to produce analogues with excellent

* Corresponding author.
E-mail address: federico.brucoli@dmu.ac.uk (F. Brucoli).

https://doi.org/10.1016/j.ejmech.2021.113734
0223-5234/

sterilizing activity against *Mycobacterium tuberculosis* (*Mtb*), improved PK/ADME parameters and reduced toxicity. As part of this drug development process, in the late 1960s the Lepetit SPA laboratories synthesised a 3-(4-methyl-1-piperazinyl)-iminomethyl derivative of rifamycin SV, rifampicin (**3**, RIF), as an orally available drug that exhibited high bactericidal activity and enhanced intestinal absorption properties (Fig. 1). RIF, which is a first-line anti-tuberculosis drug and is used in combination with isoniazid, ethambutol and pyrazinamide, was marketed in Italy in 1969 and approved by the FDA in USA in 1971 [1,4]. RIF is active against actively growing and non-replicating (dormant) *Mtb* bacilli. However, this important anti-tubercular drug has several pitfalls, including the selection of resistant mutants, if used in monotherapy, the occurrence of side effects, e.g., hepatotoxicity, and cytochrome P450 induction activity, which might result in drug-drug interaction issues.

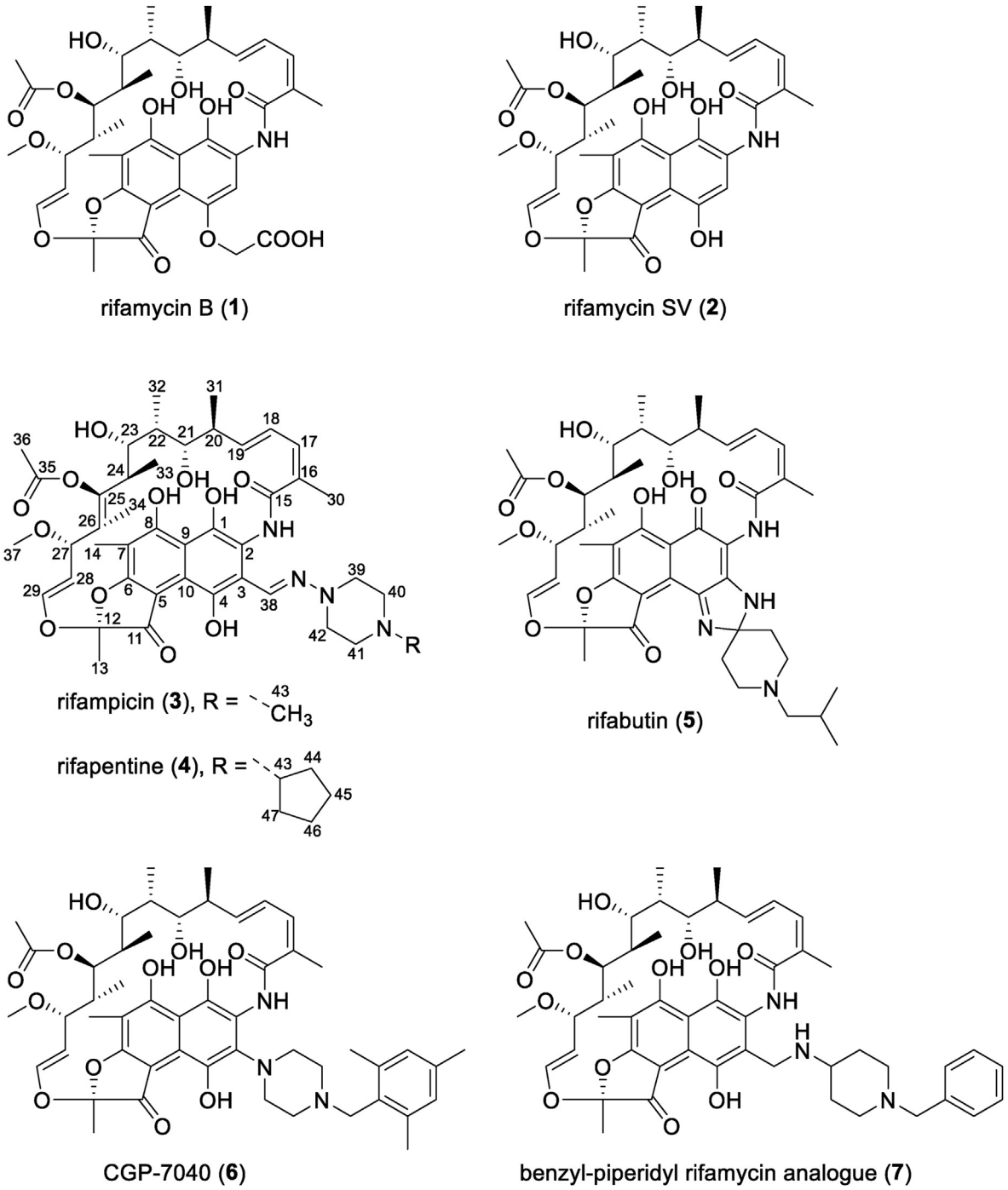

Fig. 1. Structures of rifamycin derivatives developed to treat tuberculosis infections. Rifamycin B (**1**) and SV (**2**) were originally isolated from cultures of *Amycolatopsis rifamycinica* and due to severe side effects were not developed as antibacterial dugs. Rifampicin (**3**, RIF), rifapentine (**4**, RPT) and rifabutin (**5**, RBT) are currently used to treat tuberculosis infected patients. Early rifamycin analogue CGP-7040 (**6**) had longer half-life compared to RIF and showed superior activity against non-tuberculous bacteria (e.g., MAC), although its drug development program was abandoned due to lack of financial incentives. Compound (**7**) is an experimental rifamycin SV derivative bearing a secondary amine unit that showed interesting growth inhibitory properties *in vitro* against *Mtb* H37Rv.

Other rifamycins currently used in the clinic as anti-tuberculosis drugs include rifapentine (**4**, RPT) and rifabutin (**5**, RBT). RPT (**4**) is an *N*-amino-*N*′-cyclopentanyl-piperazine derivative of rifamycin SV developed at Lepetit SPA in the late 1960s as a long-acting version of RIF (**3**) and approved by the FDA in 1998 [6]. RBT (**5**) is a spiropiperidyl-rifamycin discovered by the Achifar drug company in the mid-1970s that gained FDA approval in 1992 to treat *Mycobacterium avium* complex (MAC) disease in AIDS patients. RBT is also used to treat tuberculosis [7]. RIF, RPT and RBT are on the list of WHO essential medicines [8]. A number of earlier ryfamycins were also investigated to treat TB, including rifalazil (KRM-1648) and 3-(2,4,6-trimethylbenzylpiperazinyl)rifamycin SV (**6**, CGP-7040), although their development was terminated due to either adverse side effects in patients or shortage of drug discovery funds (Fig. 1) [9–11].

RIF (**3**) inhibits mycobacterial transcription by binding to the β-subunit of DNA-dependent RNA polymerase (RNAP). RNAP reads DNA sequences and catalyses the polymerisation of complementary RNA chains using nucleotide building-blocks, thus being ultimately responsible for the transcription and expression of mycobacterial genes [12]. The increase of resistance to RIF and RFB in *Mtb* is a result of mutations in the 81-bp area of the *rpoB* gene, termed RIF resistance-determining region (RRDR), which encodes for the β-subunit (RpoB protein) of RNA polymerase [13].

Globally, in 2019 3.3% of new TB cases and 18% of previously treated cases were either multidrug- or rifampicin-resistant tuberculosis (MDR/RR-TB), with an estimated 465 000 incident cases of RR-TB [14]. The emergence of multi-drug resistant strains and the lack of new drugs are two main factors that contribute to the re-emergence of tuberculosis.

The RNAP core enzyme (400 kDa) consists of the five subunits: α-dimer (α2), β subunit, β' subunit and ω, which form a holoenzyme and initiate transcription from promoters. RIF binds to the RNAP β-subunit, which is located near the DNA/RNA channel, by forming hydrogen bond interactions between its four hydroxyl groups at C-1, C-8, C-21, C-23 and acetoxy carbonyl oxygen at C-25, and key polymerase amino acid residues [15]. The C3-hydrophobic chain of RIF do not appear to be involved in crucial interactions at the RNAP active site and might modulate the antibiotic activity of rifamycin derivatives by improving their bacterial membrane permeation abilities [15]. RIF inhibits RNAP by steric occlusion blocking the exit of the growing RNA chain [16].

Mutations at positions 526 and 531 of the RpoB protein are generally associated with high-level of RIF resistance with high RIF MICs, whereas isolates bearing mutations at positions 516, 521, 522 and 533 exhibit moderate resistance levels to the rifamycin antibiotics RIF and RFB [17,18].

Reactions of 3-formylrifamycin SV with primary amines and amino acids [19] has been attempted in the past and several derivatives, which were modified at their C3 and C4 positions and contained amines, ketone, hydrazine and heterocyclic moieties and sulphonium and phosphonium ylides and oximes, have been prepared [20–27]. However, a focussed library of rifamycin SV derivatives bearing amino alkyl-heterocyclic chains at the C3 position has not been previously explored or screened for *Mtb* growth inhibition properties. In earlier work, benzyl moieties have been appended to either piperazinyl unit directly linked to the C-3 position of the ansa macrolide core (**6**) [9,28], or piperidyl ring attached via methylamino bridge to the rifamycin SV C-3 position [23], leading to analogues (e.g., **7**) with anti-tubercular activities against non-RR-TB *Mtb* strains comparable to that of RIF.

Here, we sought to investigate the contributions of the hydrazone linkage and methyl-piperazinyl tail of RIF to the anti-tubercular activity of the parent compound against wild-type and RR-TB *Mtb* strains. To this end, a robust reductive amination protocol was devised to incorporate at the C-3 position of rifamycin SV a small set of amino-alkyl aromatic/heteroaromatic rings that contained H-bond-accepting and -donating groups. An aminomethyl-piperazinyl-ethanol moiety was also included at the end of the C-3 alkyl tail of the macrolide to furnish a RIF-analogue (**16**) with increased hydrophilicity and a lower LogP value (4.1) compared to that of parent compound **3** ($LogP_{RIF} = 4.7$) (physicochemical properties were predicted using ACD Labs ACD/Phys Chem suite). The cleavable hydrazone unit of RIF was substituted with a more stable, protonable, secondary amino linker, which according to previous work [23], might increase intermolecular H-bond interactions and enable rifamycin analogues to resist mycobacterial inactivation via hydrolysis of their C-3 tails. As a defence mechanism against rifampicin, RIF-resistant *M. tuberculosis* strains use their enzymatic armoury to hydrolyse the hydrazone unit of the ansa antibiotic [29] and it is anticipated that the aminoalkyl linker of the novel rifamycin analogues might inhibit this inactivation process. The effectiveness of the rifamycin SV derivatives against selected RR-TB strains was measured using liquid, whole-cell phenotypic assays to determine minimum inhibitory concentrations (MIC_{90}). Interactions of the new compounds with RIF RNAP binding site were extensively investigated using molecular docking tools.

1.1. Chemistry

The reductive amination reaction of 3-formylrifamycin **7** with eight primary alkyl(aromatic) amines was carried out in a parallel synthetic fashion using sodium triacetoxyborohydride [$NaBH(OAc)_3$] as a mild and selective reducing agent (Scheme 1). Previous reductive amination attempts on the same substrate using sodium cyanoborohydride ($NaBH_3CN$) resulted in lower-yielding, slower and less clean reactions compared to $NaBH(OAc)_3$ and therefore $NaBH_3CN$ was not further pursued as the reducing agent.

The reactions proceeded smoothly, and the title compounds (**8**–**16**) were produced in medium to high yield. The presence of a protonated nitrogen atom at the C-38 position was corroborated by NMR analysis, as can be noted in the proton spectrum of **8** (Fig. 2a). This confirmed previous findings that C-3 amino linked rifamycin conjugates undergo intramolecular zwitterionisation as a result of proton transfer between the acidic naphthoquinone C-8-O*H* and C-38-nitrogen in protic solvents or in the presence of water [30,31].

The structure assignment of carbon and proton nuclei of derivative **8** are illustrated in the $^{1}H-^{13}C$ HSQC spectrum of Fig. 2b, Table S1 and Fig. S1 (HMBC spectrum).

1.2. Strains RRDR mutations analysis and antitubercular activity evaluation

The *rpoB* gene of the 65 RR-isolates examined in this study was successfully sequenced from codon 507 through 533 to identify clinically relevant mutations (Table 1). The most frequent mutation (41%) in the RpoB RRDR was found be at the 531 position, with 18 isolates bearing the S531L mutations (serine replaced by leucine). The second most frequent mutation (40%) was at position 526, with 12 isolates carrying the H526D (histidine replaced by aspartic acid). A relevant number of isolates also possessed the S522L (9%) mutation.

The novel rifamycin derivatives were screened for whole-cell growth inhibition of *M. tuberculosis* H37Rv and HN878 wild-type strains, and RR-resistant strains $RpoB_{S522L}$ $RpoB_{S531L}$ and $RpoB_{H455D}$ (HN-0258218-RM1), which was isolated as a spontaneous rifampicin resistant mutant from HN-878,[32] and minimum inhibitory concentrations (MICs) were determined at five days (Table 2). The "hypervirulent" *Mtb* HN878 was selected as it is a

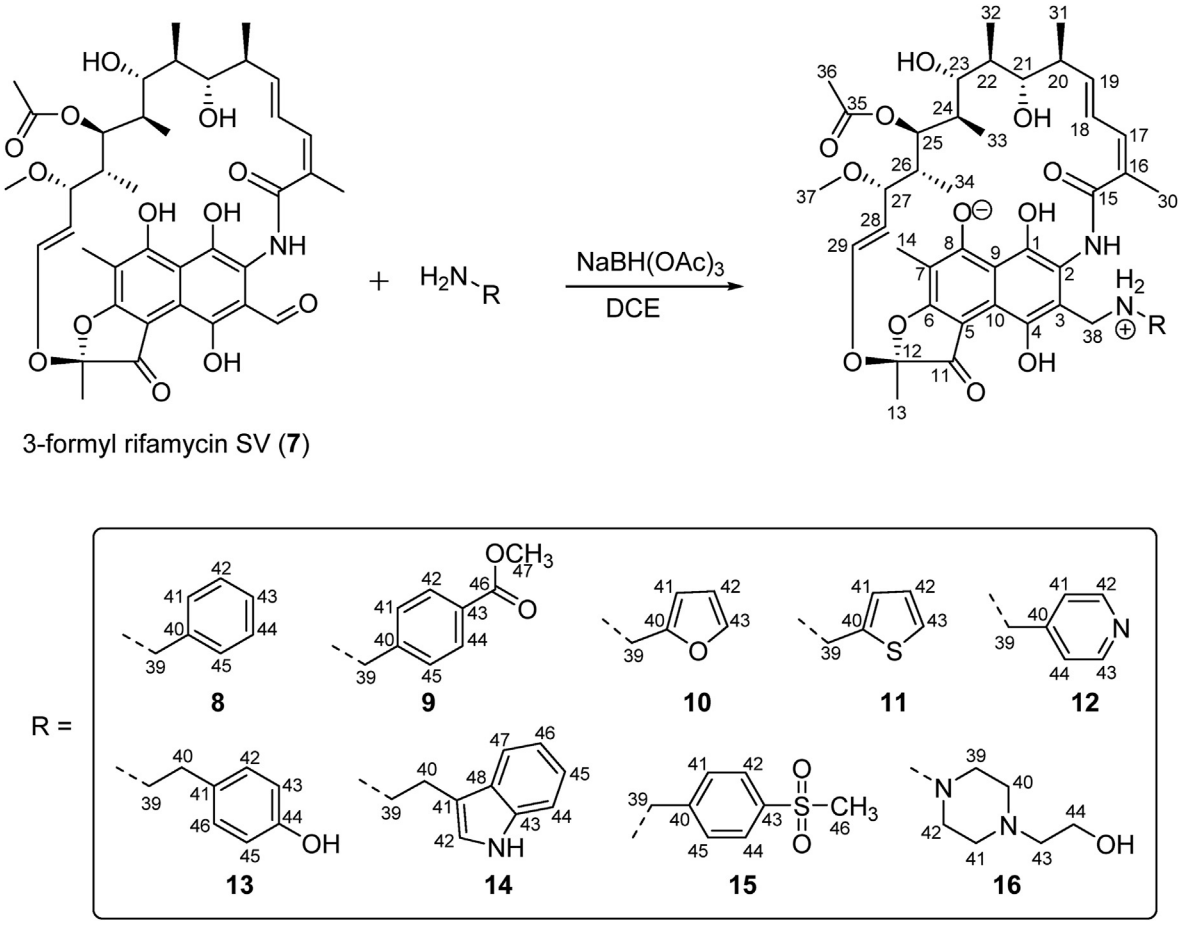

Scheme 1. Synthesis of rifamycin analogues **8**–**16**. Reagents and conditions: amines (1 equiv.), $NaBH(OAc)_3$ (1.4 equiv.), dichloroethane (DCE, 5 mL), room temperature, 3 h, 55–83% yield.

particularly insidious strain due to its ability to grow fast and drastically reduce the survival rate of immune-competent infected mice [33]. RIF-resistant strains with S531L and S522L mutations were chosen as they are generally found in isolates from a high proportion of MDR-TB patients [17].

The new rifamycin analogues **8**–**16** were active against *Mtb* H37Rv, HN-878 and $RpoB_{S522}$ RIF-resistant strains, but not against the $RpoB_{S531L}$ RR-strain. *Mtb* H37Rv was found to be the most susceptible strain to the anti-tubercular activity of the compounds. Analogues **8, 10**, **11**, **12**, **13**, **15**, **14** and **16** exhibited significant growth inhibitory properties against H37Rv with MIC values ranging from 0.034 to 0.097 μM, albeit with a 7- to 20-fold reduced potency compared to RIF (MIC = 0.0045 μM). Compounds **9** was only active at a concentration of 0.12 ± 0.046 μM, indicating that hydrogen bond acceptor groups, e.g., methyl carboxylate unit, are not well tolerated in the $RNAP_{H37Rv}$ binding pocket.

Benzylamino residue-containing analogue **8** was as effective as RIF (**3**) in killing the hypervirulent strain HN-878 with a MIC_{90} value of 0.026 ± 0.035 μM. Rifamycin derivatives **9, 10, 11, 12, 13** and **14** were less active against HN-878 compared to **8** with MIC_{90} ranging from 0.20 to 0.53 μM. Compounds **15** and **16** arrested the growth of HN-878 at concentrations of 0.096 ± 0.064 and 0.070 ± 0.042 μM, respectively. Compounds **8, 10** and **11** were active, albeit at higher concentrations (9–16 μM), against the RR strain ($RpoB_{H455D}$) isolated from HN-878.

The title compounds **8**–**16** inhibited the growth of *Mtb* $RpoB_{S522L}$ with MIC values ranging from 3 to 12 μM. Notably, analogues **14** and **15**, which contained tryptamine and methylsulfonyl-benzylamine residues, respectively, exhibited cidal activity against *Mtb* $RpoB_{S522L}$ at a concentration as low as 3.1–3.2 μM, whereas RIF was not effective against this strain (MIC >8 μM).

1.3. Molecular modelling studies

Docking studies were carried out to evaluate the binding mode of the RIF-analogues and investigate the interactions of the compounds' functional groups, including their amino-methyl aromatic tails or aminomethyl-piperazinyl-ethanol moiety (**16**), with the amino acid residues in the binding pockets of the β-subunits of wild-type (PDB ID 5UHC) [34], and S531L- and S522L-mutated RNAP enzymes. The optimized 3D structures of rifampicin analogues were docked into the RNAP binding site defined by the location of rifampicin in the complex. The resulting docking scores of the zwitterionic analogues (Table 3) indicated favourable interactions between the analogues and the amino acid residues of the RNAP. Although there is no direct correlation between the docking score and MICs of the majority of tested molecules, the molecular docking has revealed possible a novel mode of binding for the rifampicin analogues.

Molecular docking of the analogues into the rifampicin binding pocket of the wild type RNAP crystal structure (PDB ID 5UHC) indicated a possibility of three distinct modes of their interaction with RNAP (Figs. S2a–d). Most of the analogues occupied the same

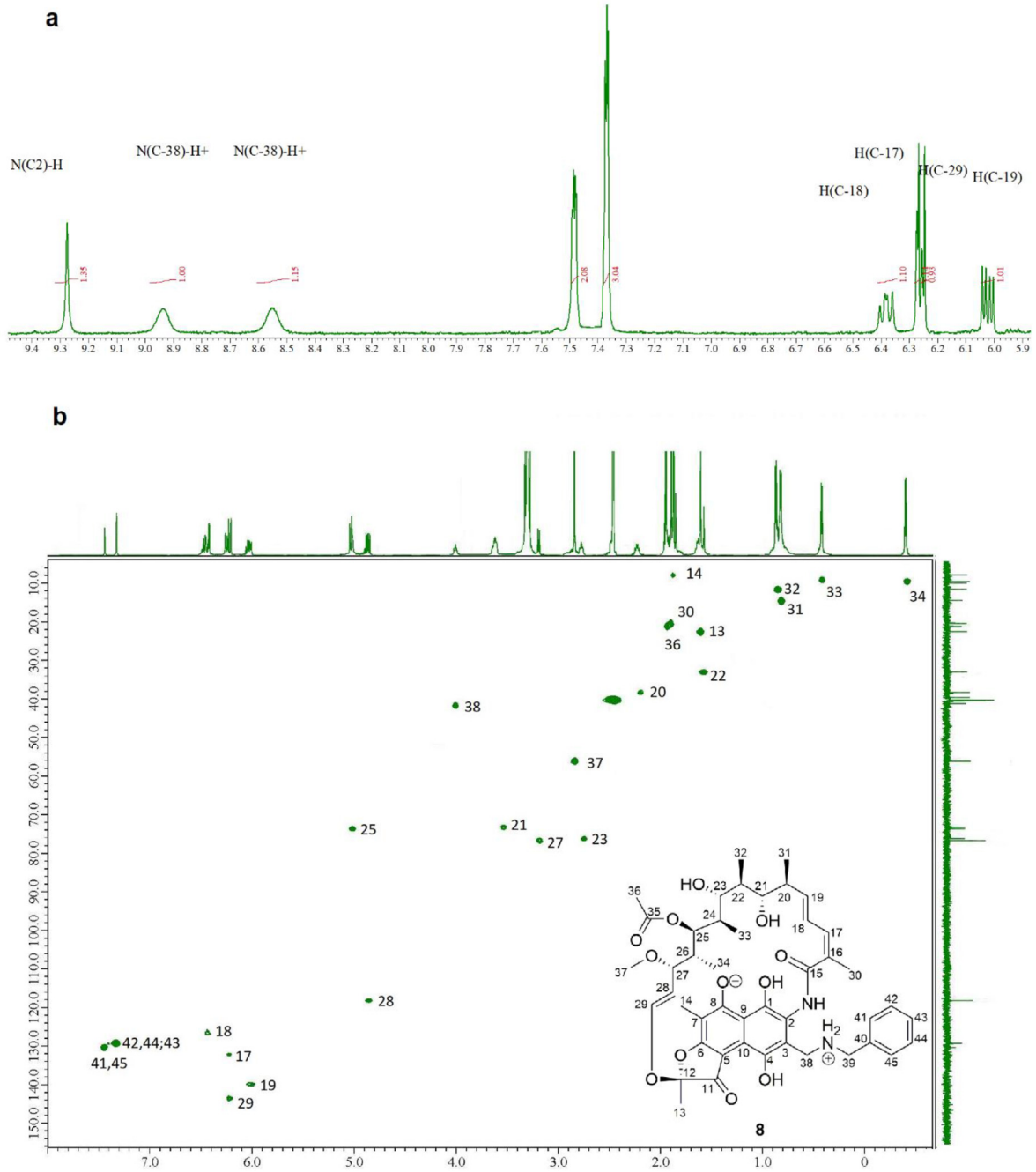

Fig. 2. a) ^{1}H NMR spectrum of 8 within the 5.9–9.5 ppm range recorded in DMSO-d_6 at 600 MHz highlighting the presence of the protonated amino group at C-38. **b)** ^{1}H– ^{13}C-HSQC spectrum of **8** in DMSO-d_6. Spectral region at δ_H −0.50 − 7.50.

space as rifampicin, with their cores overlapping with rifampicin core and different position of their tails (Fig. 3a). Consequently, these analogues form interactions with the key residues in WT RNAP similar to those observed for rifampicin [34]. In particular, hydrogen bonds were observed between those analogues and amino acids Q435, Q438, R454 and S456. Analogues **15** has a possibility to form additional hydrogen bond interactions with nucleotide and G491 (Fig. 3a).

Analogues **12** and **13** partially occupied the cavity with their cores occupying the similar space as the rifampicin tail (Fig. S2b). These analogues do not form the hydrogen bonds with the same residues despite being in close proximity, but their binding poses are stabilised by forming hydrogen bonds with R173 and F439 and via interactions with hydrophobic residue I497. While the most favourable pose of 16 partially occupied the RNAP binding site (Fig. S2c), the second pose occupied a similar space as rifampicin (Fig. S2d). Furthermore, some of the less favourable docking poses of other analogues were adopting conformations that are less deviating from the rifampicin binding mode.

There is a lack of direct correlation between the docking scores and experimentally observed activities (Tables 1 and 3), that may be due not only to different space of the binding site the ligands occupy when compared to rifampicin, but also due to their multiple conformations that can be formed within the binding site (Fig. S4).

Table 1
Sequencing of the *rpoB* gene of Rif-resistant-isolates used in this study including the numbering of the residues from the crystal structure of RNAP in complex with rifampicin (PDB ID 5UHC) [34]. The mutations that confer RR-resistance in *Mtb* are shown below the amino acid sequence of the rpoB protein. In brackets are indicated the number of isolates carrying a specific single amino acid mutation in the RNAP β-subunit.

Position	507	508	509	510	511	512	513	514	515	516	517	518	519	520	521	522	523	524	525	526	527	528	529	530	531	532	533
Position (5UHC)	432	433	434	435	436	437	438	439	440	441	442	443	444	445	446	447	448	449	450	451	452	453	454	455	456	457	458
Codons	GGC	ACC	AGC	CAG	CTG	AGC	CAA	TTC	ATG	GAC	CAG	AAC	AAC	CCG	CTG	AGC	GGC	TTG	ACC	CAC	AAG	CGC	CGA	CTG	TCG	CGC	CTG
Aminoacids	G	T	S	Q	L	S	Q	F	M	D	Q	N	N	P	L	S	G	L	T	H	K	R	R	L	S	A	L
Mutations	G (1) D (1)				P (1)		K (1)			G (1) Y (1) V (1)		Y (1)				L (6)				D (12) L (6) Y (3) R (1) P (1) N (1) A (1)					L (18) W (5) Q (1) Y (1)		

While rifampicin forms fewer conformations with one preferred, its analogues can form between 7 and 13 conformations, and some are unlikely to be bioactive. As the binding scores can be very similar, the probability of having both bioactive and inactive conformations are high, which could be one of the reasons for the lower activities of rifampicin analogues. The higher number of possible binding modes most likely results from introduction of rotatable bonds in the tails, thus increasing the flexibility of analogues. The number of torsion angles that can be changed increased from 5 in rifampicin to either 7, 8 or 9. Additionally, the higher predicted logP and lower predicted solubility of analogues, which are reflected in lower predicted drug likeness, when compared to rifampicin, may also contribute to lower biological activity (Table S2). Additionally, these difference in molecular properties may also affect the permeability of the analogues as demonstrated for a different set of rifampicin analogues [30].

Notably, rifampicin and analogues did not fully occupy the available space inside the binding site, and one of the pockets at the bottom of the cleft may be explored by the analogues (Fig. S2b). Since the protein, DNA and RNA conformations from the crystal structure may lead to biased docking results, a short molecular dynamics simulation was conducted to relax the 3D structure of the whole system. The docking of all analogues against the 3D structure extracted from the final frame of the trajectory has resulted in the docking poses that had considerable higher docking score. The careful analysis of the results indicated that the shape of the binding cavity was changed due to the change of RNA chain conformation and shrinking the space available for ligand binding. This resulted in rifampicin and all analogues interacting mainly with the RNA chain and therefore providing potentially misleading information.

Therefore, the binding of analogues with the protein only was explored by considering the 3D structure of the beta subunit on its own, an approach that was previously reported elsewhere [35]. Consequently, the structure of the beta subunit and rifampicin complex was extracted from the crystal structure file [34] and subjected to a 10 ns molecular dynamics simulation of a partially restrained protein chain that was more than 10 Å away from the rifampicin as a preparation of the protein structure for the docking. Similar to results of the docking against the whole RNAP, different binding modes were observed. The first pose of the cores of **9** and **11** occupied the similar space as rifampicin (Fig. S3a), while most analogues had their tails occupying previously unexplored space of the binding site (pocket marked with a red circle) that can be seen on the bottom left of Fig. S2b. Their cores (except 16) did not occupy the similar space as the rifampicin and have formed set of interactions with a new residue within previously unoccupied space of the RNAP binding site, namely T488 (Fig. 4a).

Finally, the reasons behind a diminished anti-tubercular activity of the analogues due to S531L mutation were explored *in silico* by replacing the serine side chain with a leucine residue at 456 position in the PDB file with RNAP crystal structure (PDB ID 5UHC) [34]. The 50 ns molecular dynamics simulation was conducted on the modified protein and the final frame of the trajectory was used as a target in the additional docking experiments. Albeit the docking scores are lower when compared to those obtained for the wild type protein, these cannot provide an explanation for the complete loss activity of these analogues and rifampicin. However, the shape of the binding site in the wild type protein appears considerably deeper than the putative binding site in the mutated protein (Fig. 5a-b). Interestingly, it can be observed that introduction of the leucine instead of serine changes the conformation on surrounding hydrophobic residues (V176, L458 and I497 in Fig. 5b). These changes not only lead to modifications to the volume, but also have a profound effect on the hydrophobicity of the cleft. This, in turn,

Table 2
Minimum inhibitory concentrations (MICs) of **8**–**16** in *M. tuberculosis* H37Rv, HN-878 and rifampicin resistant strains $RpoB_{S522L}$, $RpoB_{S531L}$ and $RpoB_{H455D}$ isolated from HN-878.

Cmp ID	*Mycobacterium tuberculosis* strains MIC_{90} (μM)[a]				
	H37Rv-LP[b]	HN-878[c]	$RpoB_{S522L}$ H37Rv[d]	$RpoB_{S531L}$[e]	$RpoB_{H455D}$[f]
8	0.097 ± 0.041	0.026 ± 0.035	12	>20	9.9
9	0.12 ± 0.046	0.53 ± 0.064	7.7	>20	>20
10	0.090 ± 0.028	0.45 ± 0.140	>20	>20	16
11	0.082 ± 0.021	0.20 ± 0.057	8	>20	14
12	0.075 ± 0.021	0.31 ± 0.140	6.7	>20	>20
13	0.066 ± 0.019	0.22 ± 0.045	5.8	>20	>20
14	0.039 ± 0.060	0.39 ± 0.010	3.1	>20	>20
15	0.039 ± 0.046	0.096 ± 0.064	3.2	>20	>20
16	0.034 ± 0.028	0.070 ± 0.042	4.7	>20	>20
RIF (3)	0.0045	0.02	>8.0	>8.0	>8.0
Isoniazid	0.28	0.29	0.29	0.55	0.62

[a] MIC_{90} was defined as the concentration required to inhibit growth of *M. tuberculosis* in liquid medium by 90% after 5 days.
[b] H37Rv (ATCC 25618 Wild-type).
[c] HN-878 wild-type.
[d] (RIF-R1) Rifampicin-resistant strain ($RpoB_{S522L}$ H37Rv-LP).
[e] (RIF-R2) Rifampicin-resistant strain ($RpoB_{S531L}$).
[f] (HN-0258218-RM1) Rifampicin-resistant strain ($RpoB_{H455D}$) isolated from HN-878. The screening was conducted in triplicate.

Table 3
Docking scores (kcal/mol) of zwitterionic **8**–**16** against *M. tuberculosis* H37Rv RpoB and rifampicin resistant strains $RpoB_{S522L}$ and $RpoB_{S531L}$ as targets. The docking scores were predicted using LeDock software. The docking score in brackets correspond to second pose.

Cmp ID	RpoB H37Rv whole system[a]	RpoB H37Rv whole system (10 ns simulated)	RpoB H37Rv β-subunit (10 ns simulated)	$RpoB_{S531L}$ H37Rv whole system (50 ns simulated)	$RpoB_{S522L}$ H37Rv β-subunit (150 ns simulated)
8	−7.9	−8.5	−6.5	−7.2	−6.8
9	−8.7	−9.2	−6.9	−8.3	−7.6
10	−7.9	−8.4	−6.4	−7.2	−6.8
11	−8.1	−8.8	−6.0	−7.4	−7.1
12	−7.8	−8.7	−6.7	−7.5	−7.0
13	−7.9	−8.7	−6.6	−7.4	−6.9
14	−8.7	−9.5	−7.4	−8.6	−7.7 (−7.7)
15	−8.5	−9.5	−7.1	−8.2	−7.8 (−7.3)
16	−7.0 (−6.8)	−9.8	−6.5	−7.9	−7.4
RIF (3)	−7.1	−8.7	−6.1	−7.4	−6.5

[a] wild type protein PDB ID 5UHC (system was not simulated prior to docking). [b] Binding score for the second pose.

has potentially a significant effect on ligand binding and can provide a structural information regarding the lack of activity against this particularly resistant strain.

Moreover, the change of the binding site shape in the protein with S522L mutation may explain the loss of anti-tubercular activity of rifampicin (**3**), the different range of activities displayed by most analogues and the increased efficacy of **15** (Fig. 5c). As the S522 (position 447 in 5UHC) is not part of the binding site, a longer molecular dynamics simulation of the mutated beta subunit was conducted, which revealed that the larger leucine side chain displaced nearby binding site residues (Fig. 5d). In particular, R454 and R613 were displaced when compared to their locations in the crystal structure [34], thus preventing formation of favourable interactions and resulting in the loss of activity of **3**. This is indicated to some extent by lower binding scores obtained for rifampicin docked against the binding site of wild type beta subunit (−8.7 kcal/mol) and S522L mutated beta protein (−7.4 kcal/mol) (Table 3). On the contrary, most of analogues retained their activity, which may be a result of their potentially different binding modes, due to their C3-aromatic tails, when compared to rifampicin. Interestingly, in addition to previously explored binding site space, tails of two most potent analogues were found to bind into a previously unoccupied space in the second most favourable poses. As illustrated in Fig. 6a, the aromatic tails of **14** and **15** nicely fitted into the space of the S522L mutated beta protein showing a favourable docking scores of −8.6 and −8.2 kcal/mol, respectively. These scores somewhat correlated with the compounds' MIC_{90} values (3.1 and 3.2 μM, respectively), which was one of the lowest of the series against $RpoB_{S522L}$ H37Rv.

These computational investigations indicate a possible rationale for the loss of rifampicin activity against resistant strains based on the changes of the binding site space as a result of amino acid mutations near the active site. However, further extended molecular dynamics simulations or crystallographic studies would be needed to confirm the exact nature of the protein structure changes resulting from the mutations of the residues that are not part of the binding site. Importantly, insights into putative mechanism of action of the rifampicin analogues were revealed and opened opportunities for optimising the activity of RNAP inhibitors. These studies provide a basis for further computer aided molecular design by targeting space previously unoccupied by rifampicin.

2. Conclusions

Mutations in *M. tuberculosis* (*Mtb*) drug targets are one of the main hurdles preventing effective treatment and management of the tuberculosis disease. Mutations in the rpoB gene encoding for the β-subunit of DNA-dependent RNA polymerase (RNAP) lead to an increased resistance in *Mtb* to rifamycin antibiotics, such as rifampicin (**3**), a first-line drug widely used for tuberculosis treatment. Extensive SAR studies previously demonstrated that the naphthohydroquinone core and hydroxyl groups attached to the

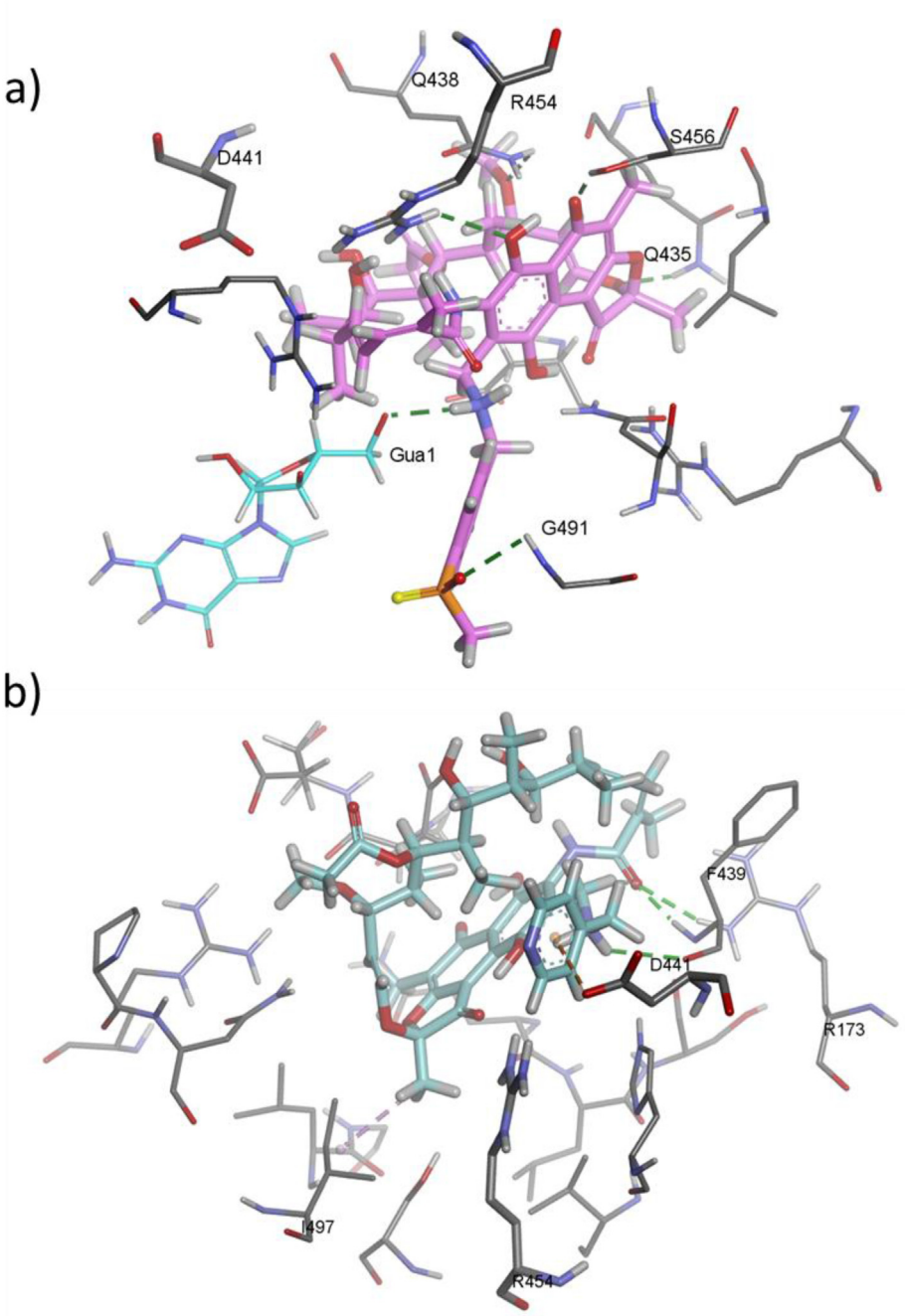

Fig. 3. a–c. Binding modes of the new rifamycin analogues within the binding pocket of the whole system of wild type *Mtb* RNAP (3D structure extracted from PDB ID: 5UHC)[34] as a target: a) **15** (pink sticks) and **12** (light blue sticks). Amino acid residues of the RNAP binding are shown as thin sticks coloured according to CPK scheme, while the carbon atoms of the nucleotide are coloured in cyan. Key residues that form interactions with the analogues are labelled, while the interactions are shown as dotted lines.

aliphatic ansa bridge of rifampicin are essential pharmacophoric characteristics enabling tight contacts with key amino acids in the RNAP β-subunit binding site. On the other hand, the 4-methyl-1-piperazinyl-iminomethyl unit of rifampicin might have a less prevalent role in establishing interactions with the binding pocket, although several authors reported different, sometimes contrasting, viewpoints on the ability of the rifampicin tail to form interactions with key residue E445 in the RNAP site [20,23,27]. It was therefore postulated that structurally diverse C3-RIF tails did not affect ligand-protein interactions but might improve the DM/PK profiles of the molecules and alter permeability of bacterial cell walls instead, leading to RIF variants with different bactericidal activity [36].

Here, in an effort to explore the contribution of C-3 tails to the anti-tubercular activities and ligand binding properties of rifamycin analogues, the piperazinyl-iminomethyl unit of rifampicin (**3**) was replaced with eight amino-alkyl-aromatic rings. The latter were connected to the naphtoquinone chromophore with a stable secondary amino linker, which in turn replaced RIF's cleavable hydrazone linkage. The resulting novel C3-(*N*-alkyl-aryl)-aminomethyl rifamycin analogues were screened against *M. tuberculosis* H37Rv and HN-878 strains, and clinical isolates bearing 522, 531 and 455 mutations. Interestingly, it was found that benzylamino-including analogue **8** was as effective as RIF (**3**) in inhibiting the

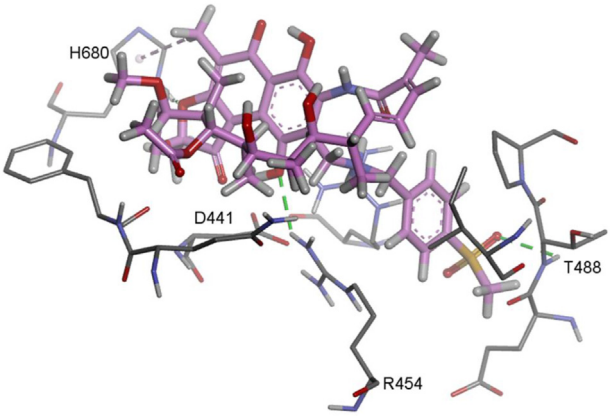

Fig. 4. Second favourable binding mode of **15** within the binding pocket of the beta subunit system of wild type *Mtb* RNAP (3D structure extracted from the molecular dynamics simulation trajectory). Carbon atoms of the analogue are coloured in pink and the amino acid residues of the RNAP binding are shown as thin sticks coloured according to CPK scheme. Key residues are labelled, while the interactions are shown as dotted lines.

growth of the hypervirulent HN-878 strain with a MIC_{90} value of 0.02 μM. The $RpoB_{H455D}$ HN-878 strain bearing a mutation outside the hotspot region of rpoB gene was also sensitive to compound **8**. Moreover, tryptamine- and methyl-sulfonyl-benzyl-containing analogues **14** and **15**, respectively, were found to be active against $RpoB_{S522L}$ H37Rv (MIC_{90} = 3 μM), whilst RIF was not effective against this strain. The S522L mutation has a high incidence in *Mtb* clinical isolates, and the scaffold of rifamycin derivatives active against strains bearing this mutation might be used for the development of more effective anti-tubercular agents.

In silico docking studies provided a possible rationale for the anti-tubercular activity of the novel analogues, which might have alternative modes of ligand interactions with the RNAP subunit. Moreover, the docking results showed that the analogues' aromatic tails might play a more prominent role in establishing molecular interactions within the binding site compared to RIF piperazine unit. Our molecular modelling experiments revealed novel binding pockets within the β-subunit that can be chemically explored by *ad hoc* designed rifampicin analogues. For example, the aromatic tails of some analogues, including **14** and **15**, were found to be positioned in a space of $RpoB_{S531L}$ binding site that was not occupied by

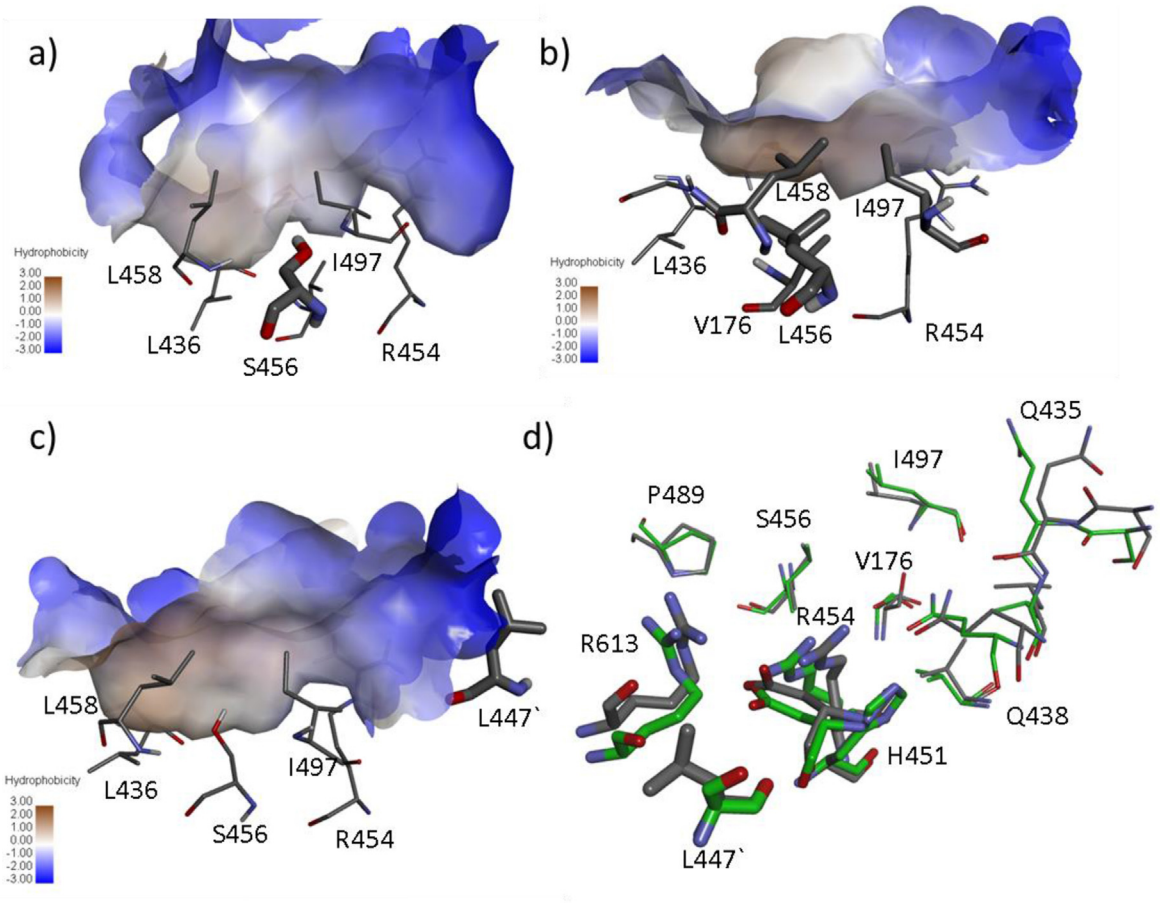

Fig. 5. a–**d**. Comparison of the rifampicin binding sites of the *Mtb* RNAP found in the: **a**) crystal structure of the wild type protein (PDB entry 5UHC), **b**) final frame of the trajectory obtained by molecular dynamics simulation of the protein with S531L mutation and **c**) final frame of the trajectory obtained by molecular dynamics simulation of the protein with S522L mutation. Binding sites are shown as spatial distribution of hydrophilicity and hydrophobicity mapped onto a surface. Most of the pocket residues are shown in thin stick representation, with S522, L522, S531 and L531 residues shown as thick sticks and selected hydrophobic residues shown as medium sticks in the mutated protein; **d**) the overlay of the residues of the binding site extracted from the crystal structure [34] (green sticks) and S522L structure (grey sticks), where the thickness of the sticks indicates the residues that affected the shape of the binding site in the mutated protein.

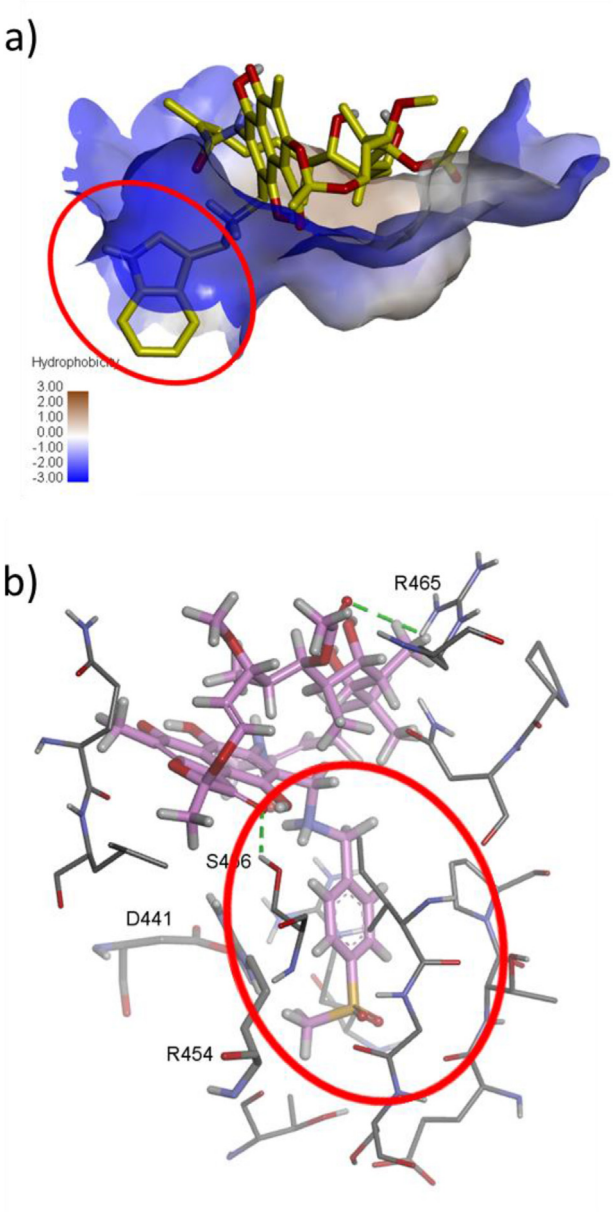

Fig. 6. a-b. The second favourable docking poses of **a**) **14** and **b**) **15** inside the binding site found in the simulated structure of S522L mutated *Mtb* RNAP. The red circle indicates unoccupied spaces of the wild type *Mtb* RNAP as an additional pocket to accommodate the tail of rifampicin analogues. The surface represents the binding site coloured according to its hydrophobicity.

the rifampicin piperazine moiety. Also, it was noted that the binding site of the $RpoB_{S531L}$ mutant strain was narrower compared to the one of the H37Rv RpoB protein, this probably occurring as direct result of the substitution of a serine with a leucine residue. In summary, this study offers an insight in the design of more active class of RIF-based anti-TB agents and highlights the role of selected C-3 appended aromatic tails in increasing the molecular interactions of rifamycin analogues with amino acid residues of the RNAP β subunit. These results might also serve as a basis for further computational studies to explain the effects of other mutations on rifampicin derivatives activities.

3. Experimental

3.1. General chemistry information

^{1}H and ^{13}C Nuclear Magnetic Resonance (NMR) spectroscopy analyses were carried out using a JEOL JNM-ECZR 600 MHz (equipped with a ROYAL probe) or Bruker Avance 400 MHz NMR spectrometers. Solvent signals for hydrogen and carbon NMR were used as the internal reference. Chemical shifts (δ_H) are quoted in parts per million and are relative to the solvents residual peaks in the ^{1}H and ^{13}C NMR spectra: $CDCl_3$ (7.26 and 77.0 ppm), MeOD-d_4 (3.31 and 49.1 ppm) and DMSO-d_6 (2.50 and 39.52 ppm). Coupling constants (J) are given in Hertz (Hz) and the signal multiplicity is described as singlet (s), doublet (d), doublet of doublets (dd), triplet of doublets (td), triplet (t), quartet (q) and multiplet (m). Chemicals were purchased from Acros Organic, Alfa Aesar, Fisher Scientific, Sigma Aldrich and VWR. The deuterated solvents ($CDCl_3$, DMSO-d_6 and MeOD-d_4) used for NMR spectroscopy experiments were purchased from Cambridge Isotope Laboratories Inc. Thin Layer Chromatography (TLC) was performed using aluminium backed 20 × 20 cm silica gel 60 F_{254}, which were purchased from Merck for viewing colourless spots under 254 nm wavelength ultraviolet light. Flash column chromatography purifications of the intermediates and final products were conducted in a glass column using irregular, 60 Å pore size silica gel, 63–200 μm, 70–230 mesh. LC-MS analysis was conducted on a Thermo Fisher – Agilent 6100 series Quadrupole LC-MS system with a G4220A 1290 binary pump/DAD. The column used was an Agilent Zorbax SB-C19 2.1 × 50 mm 1.8 μm (400 bar). Parallel synthesis was carried out using Radleys Carousel 12 Plus reaction station.

3.2. Reductive amination procedure

The aromatic primary amine (1 equiv.) was added to a solution of rifaldehyde **7** (0.1 mmol, 72.6 mg) in 1,2-dichloroethane (10 mL) and subsequently treated with sodium triacetoxyborohydride (1.4 equiv., 29.7 mg). The mixture was stirred at room temperature for 2 h under nitrogen atmosphere. After HPLC analysis showed consumption of the starting material, the reaction was quenched with 10% $NaHCO_3$ (10 mL) and the compounds extracted with EtOAc (3 × 15 mL). The organic phase was dried with $MgSO_4$ and the solvent was evaporated under reduced pressure to yield the free base as a crude reddish residue, which was purified by column chromatography using a Hexane:EtOAc/1:9 solvent system.

8. A red solid (45 mg, 55%) $R_f = 0.34$ (EtOAc - MeOH 100:1 *v/v*); MS *m/z* 817.4 (M^+1); ^{1}H NMR (600 MHz, DMSO-d_6) δ_H 9.27 (s, 1H, NH-amide), 8.93 (s, 1H, NH-amine), 8.55 (s, 1H, NH-amine), 7.49–7.48 (m, 2H, H-41/45), 7.37–7.36 (m, 3H, H-42/44, H-43), 6.40–6.36 (m, 1H, H-18), 6.27–6.26 (m, 1H, H-17), 6.26–6.24 (m, 1H, H-29), 6.02 (dd, $J = 15.9$, 7.5 Hz, 1H, H-19), 5.06 (d, $J = 11.1$ Hz, 1H, H-25), 4.90 (dd, $J = 12.8$, 8.5 Hz, 1H, H-28), 4.25–4.23 (m, 1H, H-38), 4.19 (s, 2H, H-39), 3.92 (d, $J = 9.0$ Hz, 1H, C-23-O*H*), 3.57–3.55 (m, 2H, H-21, H-38), 3.22 (d, $J = 8.7$ Hz, 1H, H-27), 2.87 (s, 3H, H-37), 2.81–2.77 (m, 1H, H-23), 2.25–2.21 (m, 1H, H-20), 1.97 (s, 3H, H-36), 1.94 (s, 3H, H-30), 1.91 (s, 3H, H-14), 1.65 (s, 3H, H-13), 1.61–1.60 (m, 1H, H-22), 1.20–1.17 (m, 1H, H-24), 0.96–0.93 (m, 1H, H-26), 0.89 (d, $J = 7.0$ Hz, 3H, H-32), 0.78 (d, $J = 7.0$ Hz, 3H, H-31), 0.39 (d, $J = 6.9$ Hz, 3H, H-33), −0.38 (d, $J = 6.8$ Hz, 3H, H-34); ^{13}C NMR (151 MHz, DMSO-d_6) δ_C 185.3 (C-11), 180.1 (C-8), 172.0 (C-6), 169.9 (C-15), 169.4 (C-35), 151.4 (C-1), 145.0 (C-4), 142.1 (C-29), 140.4 (C-19), 137.2 (C-40), 135.3 (C-17), 131.0 (C-16), 129.8 (C-41/45), 128.7 (C-42/44), 126.3 (C-18), 119.0 (C-2), 118.2 (C-28), 118.0 (C-10), 117.6

(C-9), 113.8 (C-3), 108.8 (C-12), 100.4 (C-7), 98.6 (C-5), 77.0 (C-27), 75.7 (C-23), 71.2 (C-25), 70.4 (C-21), 55.6 (C-37), 42.1 (C-38), 41.7 (C-39), 40.2 (C-26), 38.1 (C-24), 37.8 (C-20), 32.6 (C-22), 22.1 (C-13), 20.7 (C-36), 19.9 (C-30), 18.2 (C-31), 11.1 (C-32), 9.0 (C-34), 8.6 (C-33), 7.4 (C-14); HRMS: found 816.3838, calculated for $C_{45}H_{56}N_2O_{12}$ 816.3833.

9. A red solid (59 mg, 65%) $R_f = 0.25$ (EtOAc - MeOH 100:1 *v/v*); MS *m/z* 875.5 (M^+1); ^{1}H NMR (400 MHz, DMSO-d_6) δ_H 9.22 (s, 1H), 9.09 (s, 1H), 8.54 (s, 1H), 7.91 (d, $J = 8.4$ Hz, 2H), 7.64 (d, $J = 8.1$ Hz, 2H), 6.52 (d, $J = 3.1$ Hz, 1H), 6.28–6.24 (m. 1H), 6.18 (d, $J = 12.4$ Hz, 1H), 5.96 (q, $J = 7.5$ Hz, 1H), 5.05 (d, $J = 11.5$ Hz, 1H), 4.91 (dd, $J = 12.9$, 8.1 Hz, 1H), 4.33 (bs, 2H), 4.23–4.19 (m, 1H), 4.00 (d, $J = 8.3$ Hz, 1H), 3.91 (s, 3H), 3.58–3.55 (m, 1H), 3.24–3.22 (m, 1H), 2.95 (s, 1H), 2.88 (s, 3H), 2.79 (t, $J = 7.4$ Hz, 1H), 2.22–2.20 (m, 1H), 1.97 (s, 3H), 1.91 (s, 3H), 1.65 (s, 3H), 1.62 (s, 3H), 1.23 (bs, 1H), 0.88 (d, $J = 7.1$ Hz, 3H), 0.84 (d, $J = 7.4$ Hz, 3H), 0.42 (d, $J = 7.1$ Hz, 3H), −0.37 (d, $J = 6.8$ Hz, 3H); HRMS: found 874.3888, calculated for $C_{47}H_{58}N_2O_{14}$ 874.3880.

10. A red solid (60 mg, 70%) $R_f = 0.29$ (EtOAc - MeOH 100:1 *v/v*); MS *m/z* 807.1 (M^+1); ^{1}H NMR (600 MHz, DMSO-d_6) δ_H 9.27 (s, 1H), 9.01 (s, 1H), 8.57 (s, 1H), 7.67 (d, $J = 1.4$ Hz, 1H), 6.60 (d, $J = 3.4$ Hz, 1H), 6.53–6.49 (m, 1H), 6.46 (q, $J = 1.6$ Hz, 1H), 6.29 (d, $J = 10.3$ Hz, 1H), 6.25 (d, $J = 12.4$ Hz, 1H), 6.06 (q, $J = 7.8$ Hz, 1H), 5.07 (d, $J = 11.7$ Hz, 1H), 4.90 (dd, $J = 13.1$, 8.3 Hz, 1H), 4.36–4.32 (m, 1H), 4.24–4.20 (m, 2H), 3.95 (d, $J = 8.3$ Hz, 1H), 3.69–3.64 (m, 1H), 3.23 (d, $J = 9.0$ Hz, 1H), 2.94 (s, 1H), 2.88 (s, 3H), 2.81 (t, $J = 7.9$ Hz, 1H), 2.27 (q, $J = 7.8$ Hz, 1H), 1.98 (d, $J = 4.1$ Hz, 3H), 1.93 (s, 3H), 1.91 (d, $J = 3.4$ Hz, 3H), 1.65 (s, 3H), 1.61 (s, 1H), 1.23 (s, 1H), 0.91 (d, $J = 6.9$ Hz, 3H), 0.86 (d, $J = 6.9$ Hz, 3H), 0.46 (d, $J = 6.9$ Hz, 3H), −0.36 (d, $J = 6.9$ Hz, 3H); ^{13}C NMR (151 MHz, DMSO-d_6) δ_C 186.9, 184.0, 174.1, 171.4, 167.4, 154.4, 148.7, 145.3, 144.8, 143.1, 140.2, 139.2, 137.7, 131.7, 130.9, 130.1, 128.0, 126.4, 126.2, 123.0, 120.5, 116.6, 115.1, 112.5, 111.0, 108.8, 98.6, 77.9, 76.2, 73.1, 73.0, 55.6, 49.4, 42.7, 40.9, 40.2, 37.9, 37.4, 33.8, 22.0, 20.7, 19.8, 18.1, 11.1, 9.0, 8.7, 7.3; HRMS: found 806.3630, calculated for $C_{43}H_{54}N_2O_{13}$ 806.3626.

11. A red solid (72 mg, 78%) $R_f = 0.33$ (EtOAc - MeOH 100:1 *v/v*); MS *m/z* 823.4 (M^+1); ^{1}H NMR (600 MHz, DMSO-d_6) δ_H 9.23 (s, 1H), 7.62–7.58 (m, 1H), 7.26 (d, $J = 12.1$ Hz, 1H), 7.21 (d, $J = 11.4$ Hz, 1H), 6.49 (d, $J = 23.8$ Hz, 1H), 6.45 (dd, $J = 15.5$, 11.4 Hz, 0H), 6.28 (d, $J = 12.7$ Hz, 1H), 6.24 (d, $J = 12.7$ Hz, 1H), 6.04 (q, $J = 7.8$ Hz, 1H), 5.07 (d, $J = 11.0$ Hz, 1H), 4.91 (dd, $J = 12.7$, 8.3 Hz, 0H), 4.45–4.37 (m, 1H), 4.25–4.20 (m, 1H), 4.03 (q, $J = 7.1$ Hz, 1H), 3.94 (d, $J = 9.0$ Hz, 0H), 3.63 (d, $J = 12.1$ Hz, 1H), 3.25–3.23 (m, 1H), 2.89 (d, $J = 4.8$ Hz, 3H), 2.82–2.79 (m, 0H), 2.27–2.22 (m, 1H), 1.98 (d, $J = 6.4$ Hz, 3H), 1.95 (s, 3H), 1.91–1.91 (m, 3H), 1.64 (d, $J = 3.4$ Hz, 3H), 1.63 (s, 1H), 1.25–1.22 (m, 1H), 0.91 (d, $J = 6.5$ Hz, 3H), 0.83 (d, $J = 6.5$ Hz, 3H), 0.42 (d, $J = 6.9$ Hz, 3H), −0.36 (d, $J = 6.9$ Hz, 3H); ^{13}C NMR (151 MHz, DMSO-d_6) δ_C 185.1, 184.5, 172.3, 171.0, 169.6, 167.6, 149.0, 145.2, 143.3, 137.9, 135.0, 133.0, 132.3, 131.6, 128.6, 127.6, 117.7, 117.4, 116.9, 116.4, 113.8, 109.1, 108.4, 98.8, 76.6, 76.0, 73.1, 72.9, 60.0, 55.9, 42.5, 40.9, 40.3, 38.1, 37.2, 22.3, 20.9, 20.3, 18.4, 11.3, 8.9, 8.5, 7.6; HRMS: found 822.3392, calculated for $C_{43}H_{54}N_2O_{12}S$ 822.3397.

12. A red solid (65 mg, 79%) $R_f = 0.25$ (EtOAc - MeOH 100:1 *v/v*); MS *m/z* 818.3 (M^+1); ^{1}H NMR (600 MHz, DMSO-d_6) δ_H 9.24 (s, 1H), 8.74 (s, 1H), 8.61 (d, $J = 5.5$ Hz, 1H), 8.56 (d, $J = 5.5$ Hz, 2H), 7.48–7.51 (2H), 6.51 (s, 2H), 6.27 (s, 1H), 6.24 (s, 1H), 6.02 (q, $J = 7.8$ Hz, 1H), 5.09 (d, $J = 3.8$ Hz, 1H), 5.06 (d, $J = 11.0$ Hz, 1H), 4.97 (q, $J = 5.5$ Hz, 1H), 4.26 (s, 1H), 3.93 (d, $J = 9.0$ Hz, 1H), 3.58 (d, $J = 12.1$ Hz, 2H), 3.23 (d, $J = 9.0$ Hz, 1H), 3.14 (d, $J = 10.3$ Hz, 1H), 3.08 (d, $J = 10.0$ Hz, 1H), 2.88 (s, 3H), 2.82–2.78 (m, 1H), 2.25–2.20 (m, 1H), 1.99 (s, 3H), 1.98 (s, 3H), 1.91 (s, 3H), 1.65 (s, 3H), 1.23 (s, 1H), 0.90 (s, 3H), 0.88 (d, $J = 3.8$ Hz, 3H), 0.76 (d, $J = 6.9$ Hz, 3H), 0.42 (d, $J = 6.9$ Hz, 3H), −0.36 (d, $J = 6.9$ Hz, 3H); ^{13}C NMR (151 MHz, DMSO-d_6) δ_C 186.5, 183.4, 171.8, 170.8, 169.3, 150.0, 144.0, 143.0, 139.8, 139.0, 138.8, 131.9, 131.7, 130.9, 128.1, 126.3, 125.9, 124.2, 119.4, 117.9, 114.5, 108.8, 102.3, 76.3, 75.2, 73.1, 73.0, 55.6, 43.0, 40.0, 38.1, 32.5, 22.0, 20.6, 20.0, 19.8, 18.1, 11.0, 8.9, 8.6, 7.3. HRMS: found 817.3781, calculated for $C_{44}H_{55}N_3O_{12}$ 817.3786.

13. A dark red solid (68 mg, 81%) $R_f = 0.31$ (EtOAc - MeOH 100:1 *v/v*); MS *m/z* 847.3 (M^+1); ^{1}H NMR (600 MHz, DMSO-d_6) δ_H 9.28 (s, 1H), 8.40 (s, 1H), 8.27 (s, 1H), 7.02–7.00 (m, 2H), 6.71–6.67 (m, 2H), 6.33 (d, $J = 11.0$ Hz, 1H), 6.27–6.24 (m, 1H), 6.19–6.15 (m, 1H), 5.96–5.91 (m, 1H), 5.06 (d, $J = 10.7$ Hz, 1H), 4.91–4.87 (m, 1H), 4.34–4.30 (m, 1H), 4.12–4.09 (m, 1H), 4.03 (q, $J = 7.1$ Hz, 1H), 3.90 (d, $J = 9.3$ Hz, 1H), 3.73–3.67 (m, 1H), 3.09 (d, $J = 10.3$ Hz, 1H), 2.93 (m, 1H), 2.87 (s, 3H), 2.82–2.79 (m, 1H), 2.24–2.19 (m, 1H), 1.97 (s, 3H), 1.91 (s, 3H), 1.65 (m, 1H), 1.27–1.23 (m, 1H), 0.92–0.90 (m, 1H), 0.86 (dd, $J = 10.0$, 6.9 Hz, 3H), 0.81 (d, $J = 6.9$ Hz, 3H), 0.47 (d, $J = 6.2$ Hz, 3H), −0.33 (d, $J = 6.9$ Hz, 3H); ^{13}C NMR (151 MHz, DMSO-d_6) δ_C 186.6, 186.0, 172.0, 170.2, 169.5, 148.9, 144.9, 142.9, 139.0, 137.4, 136.5, 135.5, 131.7, 131.1, 130.1, 129.0, 125.9, 117.6, 117.4, 115.9, 115.1, 114.0, 108.7, 100.9, 99.5, 76.8, 74.9, 73.4, 72.9, 56.6, 47.8, 41.9, 41.2, 40.6, 38.4, 37.5, 36.5, 32.3, 22.6, 20.4, 19.2, 17.8, 11.5, 9.1, 8.9, 8.0; HRMS: found 846.3939, calculated for $C_{46}H_{58}N_2O_{13}$ 846.3936.

14. A purple-red solid (61 mg, 71%) $R_f = 0.25$ (EtOAc - MeOH 100:1 *v/v*); MS *m/z* 870.5 (M^+1); ^{1}H NMR (600 MHz, DMSO-d_6) δ_H 10.93 (s, 1H), 8.55 (bs, 1H), 7.53 (q, $J = 3.9$ Hz, 1H), 7.35 (dd, $J = 8.1$, 2.9 Hz, 1H), 7.24–7.19 (m, 1H), 7.10–7.07 (m, 1H), 7.02–6.96 (m, 1H), 6.34 (d, $J = 10.3$ Hz, 1H), 6.27–6.24 (m, 1H), 6.10–6.05 (m, 1H), 5.93–5.89 (m, 1H), 5.05–4.99 (m, 1H), 4.92 (d, $J = 12.1$ Hz, 1H), 4.39 (d, $J = 12.0$ Hz, 1H), 4.16 (d, $J = 11.0$ Hz, 1H), 3.92 (d, $J = 8.6$ Hz, 1H), 3.75 (d, $J = 12.1$ Hz, 1H), 3.69 (d, $J = 9.0$ Hz, 1H), 3.24 (d, $J = 7.9$ Hz, 1H), 3.10–3.05 (m, 1H), 2.91 (s, 3H), 2.83–2.80 (m, 1H), 2.29–2.24 (m, 1H), 1.99 (s, 3H), 1.92 (s, 3H), 1.91 (s, 3H), 1.65 (s, 3H), 1.25–1.23 (m, 1H), 1.01–0.98 (m, 1H), 0.91 (d, $J = 7.2$ Hz, 1H), 0.81 (d, $J = 6.9$ Hz, 3H), 0.30 (d, $J = 6.9$ Hz, 3H), −0.32 (d, $J = 6.9$ Hz, 3H); ^{13}C NMR (151 MHz, DMSO-d_6) δ_C 185.3, 184.9, 172.0, 170.3, 169.4, 149.2, 148.9, 144.4, 142.4, 137.8, 136.3, 132.1, 131.6, 131.4, 131.3, 126.7, 126.1, 123.2, 121.2, 118.5, 118.1, 115.2, 114.6, 111.5, 108.2, 101.3, 97.9, 76.1, 75.7, 73.2, 72.8, 55.7, 47.3, 43.0, 40.7, 40.0, 38.1, 37.8, 37.0, 32.6, 29.5, 22.0, 20.0, 19.8, 18.2, 11.1, 9.0, 8.4, 7.4; HRMS: found 869.4091 calculated for $C_{48}H_{59}N_3O_{12}$ 869.4099.

15. A red solid (65 mg, 73%) $R_f = 0.23$ (EtOAc - MeOH 100:1 *v/v*); MS *m/z* 895.4 (M^+1); ^{1}H NMR (600 MHz, DMSO-d_6) δ_H 0.24 (s, 1H), 8.74 (s, 1H), 8.56 (s, 1H), 8.00 (d, $J = 8.6$ Hz, 2H), 7.71 (d, $J = 8.6$ Hz, 2H), 6.28 (d, $J = 14.5$ Hz, 1H), 6.19–6.13 (m, 1H), 5.93 (dd, $J = 16.2$, 5.9 Hz, 1H), 5.07 (dd, $J = 10.8$, 4.6 Hz, 1H), 5.03–5.01 (m, 1H), 4.97 (dd, $J = 11.0$, 4.1 Hz, 1H), 4.90–4.86 (m, 1H), 4.17 (s, 1H), 4.05–4.02 (m, 2H), 3.90 (d, $J = 10.0$ Hz, 1H), 3.73 (d, $J = 6.5$ Hz, 1H), 3.59–3.55 (m, 1H), 3.23 (d, $J = 5.5$ Hz, 1H), 3.21 (s, 3H), 2.87 (s, 3H), 2.80 (d, $J = 5.2$ Hz, 1H), 2.25–2.18 (m, 1H), 1.99 (s, 3H), 1.94 (d, $J = 2.8$ Hz, 3H), 1.91 (s, 3H), 1.65 (d, $J = 5.9$ Hz, 3H), 1.63–1.61 (m, 1H), 1.23 (s, 1H), 0.96 (d, $J = 3.8$ Hz, 1H), 0.90 (d, $J = 7.2$ Hz, 3H), 0.80 (dd, $J = 6.7$, 1.9 Hz, 3H), 0.45 (d, $J = 6.9$ Hz, 3H), −0.36 (d, $J = 6.9$ Hz, 3H). ^{13}C NMR (151 MHz, DMSO-d_6) δ_C 185.0, 184.6, 172.0, 171.1, 168.5, 167.4, 148.9, 147.0, 146.7, 143.8, 140.4, 138.4, 137.4, 133.1, 132.7, 129.7, 129.6, 127.2, 126.0, 117.6, 117.1, 115.8, 114.9, 107.0, 101.1, 77.8, 76.1, 73.7, 72.8, 59.7, 56.8, 47.1, 43.4, 41.7, 40.0, 38.3, 33.1, 22.0, 20.6, 19.9, 18.1, 10.9, 8.8, 8.3, 7.4; HRMS: found 894.3602 calculated for $C_{46}H_{58}N_2O_{14}S$ 894.3609.

16. A dark orange solid (71 mg, 83%) $R_f = 0.32$ (EtOAc - MeOH 100:1 *v/v*); MS *m/z* 856.0 (M^+1); ^{1}H NMR (600 MHz, DMSO-d_6) δ_H 15.60 (s, 1H), 12.51 (s, 1H), 9.49 (s, 1H), 8.80 (s, 1H), 7.11 (m, 1H), 6.24 (d, $J = 10.7$ Hz, 1H), 6.20 (d, $J = 12.8$ Hz, 1H), 5.90 (dd, $J = 15.9$, 6.7 Hz, 1H), 5.35 (bs, 1H), 5.06 (d, $J = 10.7$ Hz, 1H), 5.03 (s, 1H), 4.92 (dd, $J = 12.7$, 8.1 Hz, 1H), 4.18 (d, $J = 8.8$ Hz, 1H), 3.74–3.72 (m, 1H), 3.23 (d, $J = 9.1$ Hz, 1H), 2.89 (s, 3H), 2.82 (s, 1H), 2.20–2.16 (m, 1H), 1.96 (s, 3H), 1.90 (s, 3H), 1.63 (s, 3H), 1.58 (d, $J = 7.2$ Hz, 1H), 1.34–1.30 (m, 1H), 1.05–1.00 (m, 1H), 0.88 (d, $J = 6.8$ Hz, 3H), 0.83

(d, $J = 6.8$ Hz, 3H), 0.43 (d, $J = 6.8$ Hz, 3H), −0.25 (d, $J = 6.8$ Hz, 3H). HRMS: found 854.4318 calculated for $C_{44}H_{62}N_4O_{13}$ 854.4313.

4. Microbiology

4.1. Strains and culture

M. tuberculosis strains were cultured in Middlebrook 7H9 medium plus OADC (oleic acid, albumen, dextrose, catalase) supplement and 0.05% w/v Tween 80 (7H9-OADC-Tw). Rifampicin resistant strains from three different backgrounds were used. RIF-R2 ($RpoB_{S531L}$) was obtained from ATCC (ATCC 35838). RIF-R1 ($RpoB_{S522L}$) was isolated as a spontaneous rifampicin resistant mutant from H37Rv-LP (ATCC 25618). HN-0258218-RM1 ($RpoB_{H455D}$) was isolated as a spontaneous rifampicin resistant mutant from HN-878 [32]. Strain HN878 (NR-13647) was obtained through BEI Resources, NIAID, NIH. The *rpoB* gene was sequenced in the resistant isolates to identify mutations.

4.2. Determination of minimum inhibitory concentrations

MICs were determined as previously described using OD_{590} as measurement of growth [37,38]. Briefly, compounds were tested as 10-point 2-fold serial dilutions. Bacterial growth was measured after 5 days in 7H9-OADC-Tw. Growth curves were generated using the Levenberg-Marquardt algorithm. MIC_{90} was defined as the concentration required to inhibit growth by 90% as compared to controls.

4.3. Molecular modelling

The molecular modelling work was performed using Desmond [39] with Maestro [40] as graphical user interface (GUI) ver 2020-1, AutoDock Vina ver. 1.1.2 [41] with VegaZZ ver. 3.2.1.33 [42,43] as GUI, LeDock [44], Avogadro ver 1.2.0 [45] and ChemBioOffice ver. 16.0.1.4. All the analysis and image preparations were conducted using Maestro and Discovery Studio Visualizer ver. 20.1.0.19295 [46].

The crystal structure of the wild-type *M. tuberculosis* RNAP in a complex with rifampicin (PDB ID: 5UHC) [34] was used as a target protein to investigate possible interactions of all ligands with the wild type and mutated protein $RpoB_{S522L}$. Initially, the three dimensional (3D) structures of all analogues were prepared using ChemBioOffice and saved in a. mol2 format, while the 3D structure of the wildtype RNAP was prepared using Protein Preparation Wizard implemented in Maestro by adding hydrogen atoms and setting protonation states of all ionizable groups for pH 7.

The system comprising protein in complex with rifampicin, DNA and RNA was used for further evaluations of the analogues binding in the pocket located on the beta subunit in the wild type and mutated protein. The System Builder Tool was utilized to prepare a cubic periodic solvated system using single point charge (SPC) model of water molecules, with box size 15 Å larger than a molecular system in all directions. Adequate number of Na^+ and Cl^- ions were added to neutralize the system and mimic conditions with 0.05 M NaCl concentration. Additionally, following previously reported study structure where it was demonstrated that each subunit is relatively independent and that only β subunit be simulated [35], the β subunit in complex with rifampicin was extracted. The truncated system was prepared in the same way as the full system described as above.

Initially, the default Desmond "Molecular Dynamics" protocol and OPLS2005 all atoms force field for that include minimization, equilibration and production run steps was used to conduct simulations for 10 ns. Temperature was kept constant at 300 K with the Nose-Hoover thermostats and pressure was maintained with the Martyna–Tobias–Klein barostats within the NPT ensemble [47]. The cut off value of 9.0 Å was set in calculations of van der Waals and short-range coulombic interactions. The equation of motion was solved with the RESPA integrator, with an inner time step of 2.0 fs and an outer time step of 6.0 fs. [48]. The results were saved as trajectory by storing coordinates and the energies to disk at every 5 ps. The 10 ns MD simulation was carried out to relax the protein and use the final frame of the trajectory as the target structure of the wild type protein for further docking.

In the truncated systems, the large conformational change was observed for the protein segment of residues between I1041and E1153 that resulted in formation of undesired intermolecular protein interactions and unrealistic binding pocket. Therefore, positional restraints with a force constant of 50 kcal mol^{-1} $Å^{-2}$ were applied for all atoms that were away more than 10 Å from bound rifampicin. The 10 ns MD simulation was repeated to relax the protein and use the final frame of the trajectory as the target structure of the wild-type protein for further docking.

The final frames of the resulting trajectories were also used to generate 3D structures of the full system with a S531L mutation and only β subunit with a S522L mutation. Maestro function "Mutate residue" was used to change the serine residues (residue numbers 447 and 456 in the 5UHC entry) into leucine. The modified protein systems were subjected to the protocol for building solvated systems and prepared for the molecular dynamics simulation using the same procedure and settings as for the systems containing wild type structure. Additional 50 ns of the full system and 150 ns of the truncated system production runs NPT simulations were conducted to explore possible effects of mutation on the interactions of residues from the binding site with the rifampicin and analogues. The final frame of the extended simulation trajectories were extracted and used as a target in the molecular docking.

The 3D structures of rifampicin analogues were initially built by modifying the previously determined X-ray structure of zwitterionic analog of rifampicin [49]. These structures were further fully optimized using MOPAC software and PM7 Hamiltonian [50], and saved as mol2. The protein structures extracted from crystal structure (PDB ID 5UHC) [34] and final frames of the trajectories were used as targets in the docking with the binding sites positioned in the geometrical centers of a bound rifampicin. The docking of ligands in zwitterionic form was conducted using LeDock software. The center of the 20 Å × 20 Å × 20 Å box was positioned on the rifampicin ligand and 20 poses were generated for each analogue. The additional Root Mean Square Deviation (RMSD) cutoff of 1 Å was set to redundancy of poses. The reliability of the docking simulations was demonstrated by redocking rifampicin into the binding site and reproducing the binding modes of the ligand crystal structure within RMSD of 0.7 Å. The largest change of the molecule was observed for piperazine moiety as it is highly dependent on the RNA conformation that changes during the molecular dynamics simulation.

Funding

No funding was received for this work.

Declaration of competing interest

The authors declare that they have no known competing financial interests or personal relationships that could have appeared to influence the work reported in this paper.

Acknowledgment

Kyle Krieger and Renee Allen are thanked for technical assistance.

Appendix A. Supplementary data

NMR spectral data for **8**–**16**. Molecular docking scores for rifampicin analogues against *M. tuberculosis* H37Rv RpoB and images showing the binding modes of selected analogues within the binding pocket of the β-subunit of wild-type *M. tuberculosis* RNAP.

Supplementary data to this article can be found online at https://doi.org/10.1016/j.ejmech.2021.113734.

References

[1] P. Sensi, P. Margalith, M.T. Timbal, Rifomycin, a new antibiotic; preliminary report, Farmaco. [Sci.] 14 (1959) 146.
[2] T.D. McHugh, Tuberculosis: Diagnosis and Treatment; Cabi, vol. 21, 2013.
[3] W. Rifampin Lester, A semisynthetic derivative of rifamycin-A prototype for the future, Annu. Rev. Microbiol. 26 (1972) 85–102.
[4] P. Sensi, History of the development of rifampin, Rev. Infect. Dis. 5 (1983) S402–S406.
[5] N. Maggi, C.R. Pasqualucci, R. Ballotta, P. Sensi, Rifampicin: a new orally active rifamycin, Chemotherapy 11 (1966) 285–292.
[6] V. Arioli, M. Berti, G. Carniti, E. Randisi, E. Rossi, R. Scotti, Antibacterial activity of DL 473, a new semisynthetic rifamycin derivative, J. Antibiot. 34 (1981) 1026–1032.
[7] R.J. O'Brien, M.A. Lyle, D.E. Snider Jr., Rifabutin (ansamycin LM 427): a new rifamycin-S derivative for the treatment of mycobacterial diseases, Rev. Infect. Dis. 9 (1987) 519–530.
[8] World Health Organization No title, World Health Organization Model List of Essential Medicines: 21st List 2019, 2019.
[9] N. Lounis, G. Roscigno, In vitro and in vivo activities of new rifamycin derivatives against mycobacterial infections, Curr. Pharmaceut. Des. 10 (2004) 3229–3238.
[10] P.A. Aristoff, G.A. Garcia, P.D. Kirchhoff, H.H. Showalter, Rifamycins–obstacles and opportunities, Tuberculosis 90 (2010) 94–118.
[11] W.A. Vischer, P. Imhof, S. Hauffe, P. Degen, Pharmokinetics of new long-acting rifamycin-derivatives in man, Bull. Int. Union Tuberc. 61 (1986) 8.
[12] S. Ramaswamy, J.M. Musser, Molecular genetic basis of antimicrobial agent resistance in Mycobacterium tuberculosis: 1998 update, Tuber. Lung Dis. 79 (1998) 3–29.
[13] A.N. Unissa, L.E. Hanna, Molecular mechanisms of action, resistance, detection to the first-line anti tuberculosis drugs: rifampicin and pyrazinamide in the post whole genome sequencing era, Tuberculosis 105 (2017) 96–107.
[14] World Health Organization, Global Tuberculosis Report 2019, World Health Organization, Geneva (Switzerland), 2020, 2020.
[15] E.A. Campbell, N. Korzheva, A. Mustaev, K. Murakami, S. Nair, A. Goldfarb, S.A. Darst, Structural mechanism for rifampicin inhibition of bacterial RNA polymerase, Cell 104 (2001) 901–912.
[16] A. Feklistov, V. Mekler, Q. Jiang, L.F. Westblade, H. Irschik, R. Jansen, A. Mustaev, S.A. Darst, R.H. Ebright, Rifamycins do not function by allosteric modulation of binding of Mg2+ to the RNA polymerase active center, Proc. Natl. Acad. Sci. U.S.A. 105 (2008) 14820–14825.
[17] Z.L. Berrada, S.G. Lin, T.C. Rodwell, D. Nguyen, G.F. Schecter, L. Pham, J.M. Janda, W. Elmaraachli, A. Catanzaro, E. Desmond, Rifabutin and rifampin resistance levels and associated rpoB mutations in clinical isolates of Mycobacterium tuberculosis complex, Diagn. Microbiol. Infect. Dis. 85 (2016) 177–181.
[18] F.B. Jamieson, J.L. Guthrie, A. Neemuchwala, O. Lastovetska, R.G. Melano, C. Mehaffy, Profiling of *rpoB* mutations and MICs for rifampin and rifabutin in Mycobacterium tuberculosis, J. Clin. Microbiol. 52 (2014) 2157.
[19] D. Czerwonka, J. Domagalska, K. Pyta, M.M. Kubicka, P. Pecyna, M. Gajecka, P. Przybylski, Structure–activity relationship studies of new rifamycins containing l-amino acid esters as inhibitors of bacterial RNA polymerases, Eur. J. Med. Chem. 116 (2016) 216–221.
[20] K. Pyta, A. Janas, M. Szukowska, P. Pecyna, M. Jaworska, M. Gajecka, F. Bartl, P. Przybylski, Synthesis, docking and antibacterial studies of more potent amine and hydrazone rifamycin congeners than rifampicin, Eur. J. Med. Chem. 167 (2019) 96–104.
[21] K. Pyta, P. Przybylski, B. Wicher, M. Gdaniec, J. Stefańska, Intramolecular proton transfer impact on antibacterial properties of ansamycin antibiotic rifampicin and its new amino analogues, Org. Biomol. Chem. 10 (2012) 2385–2388.
[22] K. Pyta, P. Przybylski, K. Klich, J. Stefańska, A new model of binding of rifampicin and its amino analogues as zwitterions to bacterial RNA polymerase, Org. Biomol. Chem. 10 (2012) 8283–8297.
[23] K. Pyta, K. Klich, J. Domagalska, P. Przybylski, Structure and evaluation of antibacterial and antitubercular properties of new basic and heterocyclic 3-formylrifamycin SV derivatives obtained via 'click chemistry'approach, Eur. J. Med. Chem. 84 (2014) 651–676.
[24] R. Cricchio, G. Tamborini, P. Bravo, G. Gaudiano, The reaction of 3-formylrifamycin SV with sulphonium and phosphonium ylides, Farmaco. [Sci.] 29 (1974) 358–365.
[25] M. Taguchi, N. Aikawa, G. Tsukamoto, Reaction of 3-formylrifamycin S with secondary amines, Chem. Pharm. Bull. 32 (1984) 4388–4395.
[26] K. Bujnowski, L. Synoradzki, T.A. Zevaco, E. Dinjus, E. Augustynowicz-Kopeć, A. Napiorkowska, Rifamycin antibiotics—new compounds and synthetic methods. Part 4: study of the reaction of 3-formylrifamycin SV with secondary amines and ketones, Tetrahedron 71 (2015) 158–169.
[27] S.K. Gill, H. Xu, P.D. Kirchhoff, T. Cierpicki, A.J. Turbiak, B. Wan, N. Zhang, K. Peng, S.G. Franzblau, G.A. Garcia, Structure-based design of novel benzoxazinorifamycins with potent binding affinity to wild-type and rifampin-resistant mutant Mycobacterium tuberculosis RNA polymerases, J. Med. Chem. 55 (2012) 3814–3826.
[28] J.M. Dickinson, D.A. Mitchison, In vitro activity of new rifamycins against rifampicin-resistant M. tuberculosis and MAIS-complex mycobacteria, Tubercle 68 (1987) 177–182.
[29] H.G. Floss, T. Yu, Rifamycin mode of action, resistance, and biosynthesis, Chem. Rev. 105 (2005) 621–632.
[30] K. Pyta, A. Janas, N. Skrzypczak, W. Schilf, B. Wicher, M. Gdaniec, F. Bartl, P. Przybylski, Specific interactions between rifamycin antibiotics and water influencing ability to overcome natural cell barriers and the range of antibacterial potency, ACS Infect. Dis. 5 (2019) 1754–1763.
[31] K. Pyta, P. Przybylski, F. Bartl, Regioselective long-range proton transfer in new rifamycin antibiotics: a process in which crown ethers act as stronger Brønsted bases than amines, ChemPhysChem 16 (2015) 938–942.
[32] T.R. Ioerger, T. O'Malley, R. Liao, K.M. Guinn, M.J. Hickey, N. Mohaideen, K.C. Murphy, H.I. Boshoff, V. Mizrahi, E.J. Rubin, Identification of new drug targets and resistance mechanisms in Mycobacterium tuberculosis, PLoS One 8 (2013), e75245.
[33] C. Manca, L. Tsenova, A. Bergtold, S. Freeman, M. Tovey, J.M. Musser, C.E. Barry, V.H. Freedman, G. Kaplan, Virulence of a Mycobacterium tuberculosis clinical isolate in mice is determined by failure to induce Th1 type immunity and is associated with induction of IFN-α/β, Proc. Natl. Acad. Sci. U.S.A. 98 (2001) 5752–5757.
[34] W. Lin, S. Mandal, D. Degen, Y. Liu, Y.W. Ebright, S. Li, Y. Feng, Y. Zhang, S. Mandal, Y. Jiang, Structural basis of Mycobacterium tuberculosis transcription and transcription inhibition, Mol. Cell. 66 (2017) 169–179, e8.
[35] Q. Zhang, S. Tan, T. Xiao, H. Liu, S.J.A. Shah, H. Liu, Probing the molecular mechanism of rifampin resistance caused by the point mutations S456L and D441V on Mycobacterium tuberculosis RNA polymerase through Gaussian accelerated molecular dynamics simulation, Antimicrob. Agents Chemother. (2020) 64.
[36] I. Artsimovitch, M.N. Vassylyeva, D. Svetlov, V. Svetlov, A. Perederina, N. Igarashi, N. Matsugaki, S. Wakatsuki, T.H. Tahirov, D.G. Vassylyev, Allosteric modulation of the RNA polymerase catalytic reaction is an essential component of transcription control by rifamycins, Cell 122 (2005) 351–363.
[37] T.R. Ioerger, Y. Feng, K. Ganesula, X. Chen, K.M. Dobos, S. Fortune, W.R. Jacobs Jr., V. Mizrahi, T. Parish, E. Rubin, C. Sassetti, J.C. Sacchettini, Variation among genome sequences of H37Rv strains of *Mycobacterium tuberculosis* from multiple laboratories, J. Bacteriol. 192 (14) (2010) 3645–3653.
[38] J. Ollinger, M.A. Bailey, G.C. Moraski, A. Casey, S. Florio, T. Alling, M.J. Miller, T. Parish, A Dual read-out assay to evaluate the potency of compounds active against *Mycobacterium tuberculosis*, PLoS One 8 (2013), e60531.
[39] K.J. Bowers, D.E. Chow, H. Xu, R.O. Dror, M.P. Eastwood, B.A. Gregersen, J.L. Klepeis, I. Kolossvary, M.A. Moraes, F.D. Sacerdoti, In scalable algorithms for molecular dynamics simulations on commodity clusters, in: SC'06: Proceedings of the 2006 ACM/IEEE Conference on Supercomputing, IEEE, 2006, p. 43.
[40] D. E. Shaw Research, New York, NY, Schrödinger Release 2020-1: Desmond Molecular Dynamics System, Maestro-Desmond Interoperability Tools, Schrödinger, New York, NY, 2020, 2020.
[41] O. Trott, A.J. Olson, AutoDock Vina, Improving the speed and accuracy of docking with a new scoring function, efficient optimization, and multithreading, J. Comput. Chem. 31 (2010) 455–461.
[42] A. Pedretti, L. Villa, G. Vistoli, VEGA–an open platform to develop chemo-bioinformatics applications, using plug-in architecture and script programming, J. Comput. Aided Mol. Des. 18 (2004) 167–173.
[43] A. Pedretti, L. Villa, G. Vistoli, VEGA: a versatile program to convert, handle and visualize molecular structure on Windows-based PCs, J. Mol. Graph. Model. 21 (2002) 47–49.
[44] N. Zhang, H. Zhao, Enriching screening libraries with bioactive fragment space, Bioorg. Med. Chem. Lett 26 (2016) 3594–3597.
[45] M.D. Hanwell, D.E. Curtis, D.C. Lonie, T. Vandermeersch, E. Zurek, G.R. Hutchison, Avogadro: an advanced semantic chemical editor, visualization, and analysis platform, J. Cheminf. 4 (2012) 1–17.
[46] Dassault Systèmes BIOVIA, Discovery Studio Modeling Environment, Release, Dassault Systèmes, San Diego, 2017, 2016.
[47] W.G. Hoover, Canonical dynamics: equilibrium phase-space distributions, Phys. Rev. A 31 (1985) 1695.
[48] D.D. Humphreys, R.A. Friesner, B.J. Berne, A multiple-time-step molecular dynamics algorithm for macromolecules, J. Phys. Chem. 98 (1994)

6885–6892.
[49] B. Wicher, K. Pyta, P. Przybylski, E. Tykarska, M. Gdaniec, Redetermination of rifampicin pentahydrate revealing a zwitterionic form of the antibiotic, Acta Crystallogr. C 68 (5) (2012) o209–o212, https://doi.org/10.1107/S0108270112015296.
[50] J.J. Stewart, Optimization of parameters for semiempirical methods VI: more modifications to the NDDO approximations and re-optimization of parameters, J. Mol. Model. 19 (1) (2013) 1–32, https://doi.org/10.1007/s00894-012-1667-x.